Particle Dynamics in a Diblock-Copolymer-Based Dodecagonal Quasicrystal and Its Periodic Approximant by X-Ray Photon Correlation Spectroscopy

Andreas J. Mueller,[1] Aaron P. Lindsay,[1] Ronald M. Lewis III,[2] Qingteng Zhang,[3] Suresh Narayanan,[3]
Timothy P. Lodge,[1,4] Mahesh K. Mahanthappa,[1,*] and Frank S. Bates[1,†]

[1]*Department of Chemical Engineering and Materials Science, University of Minnesota, Minneapolis, Minnesota 55455, USA*
[2]*Infineum USA, Linden, New Jersey 07036, USA*
[3]*Advanced Photon Source, Argonne National Laboratory, Lemont, Illinois 60349, USA*
[4]*Department of Chemistry, University of Minnesota, Minneapolis, Minnesota 55455, USA*

Temperature-dependent x-ray photon correlation spectroscopy (XPCS) measurements are reported for a binary diblock-copolymer blend that self-assembles into an aperiodic dodecagonal quasicrystal and a periodic Frank-Kasper σ phase approximant. The measured structural relaxation times are Bragg scattering wavevector independent and are 5 times faster in the dodecagonal quasicrystal than the σ phase, with minimal temperature dependence. The underlying dynamical relaxations are ascribed to differences in particle motion at the grain boundaries within each of these tetrahedrally close-packed assemblies. These results identify unprecedented particle dynamics measurements of tetrahedrally coordinated micellar block polymers, thus expanding the application of XPCS to ordered soft materials.

Comparatively little work has addressed the symmetry-dependent particle dynamics in self-assembled soft materials, particularly tetrahedrally close-packed Frank-Kasper (FK) phases [1–6] and related quasicrystals [7–11]. Originally discovered in metal alloys [12–14], aperiodically ordered quasicrystals display local rotational symmetries with no long-range translational order. Recent experiments and simulations on metallic dodecagonal quasicrystals (DDQCs) exposed the importance of particle and grain boundary dynamics in polycrystalline configurations [15], and TEM imaging revealed phason dynamics in a decagonal Al-Cu-Co quasicrystal [16]. Complementary studies of particle-forming soft materials identify DDQCs as metastable intermediates relative to equilibrium FK phases, such as the 3D periodic σ phase [8,10,17], both of which exhibit similar arrangements of 2D square and triangle tiling motifs [18]. The latter reports primarily focused on the static structures of these complex assemblies, with only limited insight into the constituent particle dynamics by dynamic mechanical spectroscopy (DMS) [3,8], which convolves relaxation processes across many length scales. Thus, the explicit impacts of aperiodic and periodic mesostructural symmetries on the underlying micelle dynamics therein are unknown.

X-ray photon correlation spectroscopy (XPCS) offers exciting opportunities to reveal dynamic information as a function of the scattering wavevector ($\boldsymbol{q}$) at nanometer length scales, which has motivated XPCS studies of disordered [19,20] and ordered block copolymer melts [21,22]. Recently, a particle-forming polystyrene-*block*-1,4-polybutadiene (SB) diblock-copolymer melt was characterized in the supercooled disordered liquidlike packing (LLP) [23] and body-centered cubic (bcc) ordered states [24]. This work crucially hinged on a new analytical framework for handling significant intensity variations at a given q value (i.e., azimuthally anisotropic scattering) characteristic of ordered polycrystalline materials [25]. This report expands the application of XPCS to a single binary SB diblock-copolymer blend that forms both aperiodic DDQC and 3D periodic σ phases under different thermal processing conditions, revealing strikingly different dynamic signatures that characterize these low symmetry particle packings.

This study focuses on a blend of SB19 ($M_n = 30$ kg/mol, $f_B = 0.19$, $Đ = 1.02$) and SB49 ($M_n = 27$ kg/mol, $f_B = 0.49$, $Đ = 1.01$) with an SB19 volume fraction of $\varphi_{SB19} = 0.125$. These polymers were synthesized by anionic polymerization as reported previously [26]. The blend, denoted SB-B, has an average B-volume fraction $\langle f_B \rangle = 0.23$, and an order-disorder transition temperature $T_{ODT} = 180\,°C$. The full phase portrait for this blend system is presented in Supplemental Material, Fig. S1 [27–37].

SB-B powder was sealed in an aluminum sample cell in a glovebox under argon at $150\,°C$ to prevent oxidative degradation during extended high temperature annealing. Sample thermal history imprinted during this loading procedure was erased by heating the sealed SB-B sample to $200\,°C$ for 5 min prior to quenching in room-temperature tap water, vitrifying the matrix S block and trapping a metastable disorganized LLP state. The sample cell was then loaded into a temperature-controlled sample holder at
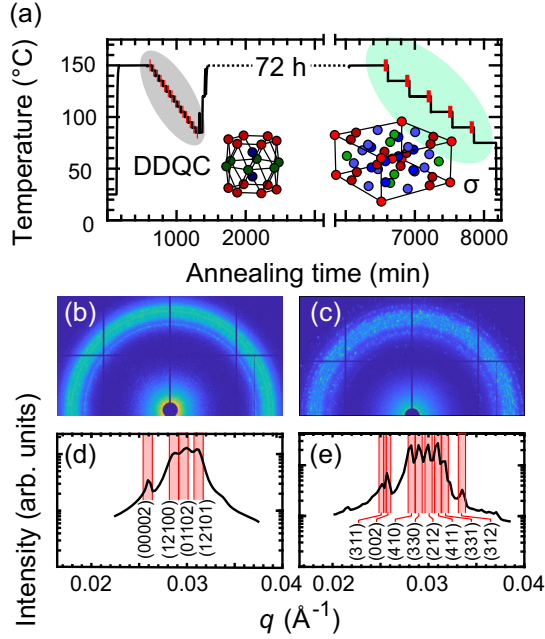
FIG. 1. (a) Thermal treatment of SB-B to form DDQC and σ phases for XPCS studies. The dotted line from $\sim$1500 s to $\sim$6000 s refers to a 72 h off-beam isothermal annealing step at 150 °C. (b)–(e) 2D-SAXS detector images and corresponding 1D-SAXS traces for (b),(d) DDQC and (c),(e) σ. Shaded boxes labeled with (hkl) reflections in (d),(e) correspond to the Δq slices in which XPCS analyses were performed.

the x-ray beamline at 150 °C establishing the $t = 0$ min point in the thermal history diagram in Fig. 1(a).

Time-resolved coherent small angle x-ray scattering (SAXS) measurements subject to XPCS analysis were performed at Sector 8-ID-I at the Advanced Photon Source (Argonne, IL). SAXS patterns were collected on a LAMBDA 750K 2D pixel array detector, with an incident wavelength $\lambda = 1.14$ Å, and a 4.000 m sample-to-detector distance. To minimize sample beam damage while maximizing scattered x-ray intensity and experimental time frames, two measurement protocols of varying frame rate and exposure time were used. For the DDQC measurement, raw XPCS data comprised 1000 detector images (frames) collected at a frequency of 1 Hz with a 1 s exposure time, totaling 16.7 min per measurement with 200 s of x-ray exposure. For the σ phase, 3600 frames were collected at a frequency of 1 Hz with a 0.1 s exposure time every second for a total experiment time of 60 min and 1800 s of x-ray exposure; note the reduced x-ray exposure time was supplemented with greater beam attenuation to counteract the higher x-ray dose. Sample stability measurements presented in Supplemental Material, Fig. S2 [27] confirm that no substantial degradation occurred during measurement, evidenced by a stable total SAXS intensity captured in each acquired frame. In each protocol, the x-ray spot size was 15 μm × 15 μm; a 0.5 mm sample thickness yields a total illuminated sample volume of 112 500 μm³. Structural

assignments of σ or DDQC phases were made by indexing time-averaged 1D-SAXS profiles, plotted in terms of scattered intensity versus scattering wavevector magnitude $|\mathbf{q}| = q = 4\pi\lambda^{-1}\sin(\theta/2)$, where θ is the scattering angle, to the known space group symmetries [3,8].

After 10 h at 150 °C, SB-B developed no crystallographic order, motivating XPCS measurements made during a cooling ramp indicated by the step pattern highlighted in the gray oval centered on 1000 min in Fig. 1(a). Sample temperature was reduced in 5 °C steps at 20 °C/min with 25 min of equilibration and 16.7 min of measurement at each temperature according to the DDQC measurement protocol (1000 frames, 1 Hz frequency, 1 s exposure). This cooling ramp induced rapid DDQC formation starting at 145 °C, evidenced by representative 135 °C 2D [Fig. 1(b)] and 1D [Fig. 1(d)] time-averaged SAXS patterns. The indexed, azimuthally integrated 1D-SAXS trace in Fig. 1(d) displays four characteristic reflections of the DDQC aligning with the established five-dimensional indexing scheme $(h_1h_2h_3h_4h_5)$ [26], which reveals an in-plane particle center-to-center distance (square-triangle tile edge length, *vide infra*) $a = 47.5$ nm within the aperiodically ordered layers with a periodic layer spacing $c = 48.5$ nm.

Following XPCS measurement of the SB-B DDQC, the sample was removed from the beamline and annealed on a hotplate at 150 °C for 72 h, replaced into the *in situ* temperature-controlled environment at 150 °C, and another cooling ramp down to 105 °C was performed now with dwell and measurement times of 5 h and 1 h, respectively, at each temperature under the σ XPCS protocol (3600 frames, 1 Hz, 0.1 s exposure). The cooling rate during this second ramp was 20 °C/min during each temperature change. SB-B produced SAXS patterns similar to those shown for 135 °C in Figs. 1(c) and 1(e), indexing to the $P4_2/mnm$ symmetry space group of a FK σ phase with lattice parameters $a = 92.1$ nm and $c = 48.9$ nm, and an average total particle radius (core and corona) $R = 14.9$ nm. The close agreement between the c-axis layer spacings of σ and DDQC implies the expected shared particle size across both structures.

Intensity-intensity autocorrelation functions, $g_2(q,\varphi,dt)$, with azimuthal angle (φ) and frame time spacing (dt) were calculated from frames collected for each structure at each temperature. Regions of the 2D-SAXS patterns corresponding to different structural features of each sample were binned and averaged together. The 2D-detector image obtained from the SB-B DDQC phase [Fig. 1(b)] exhibits a nearly isotropic powder diffraction pattern with minimal azimuthal (in φ) intensity variations. Accordingly, intensity autocorrelation analyses for the DDQC were performed using an established multi-τ algorithm [38,39] at four discrete q values corresponding to the prominent Bragg reflections in Fig. 1(d), averaged over φ with a peak-ring width of $\Delta q = 0.001$ Å^{-1}, yielding $g_2(q,dt)$ results
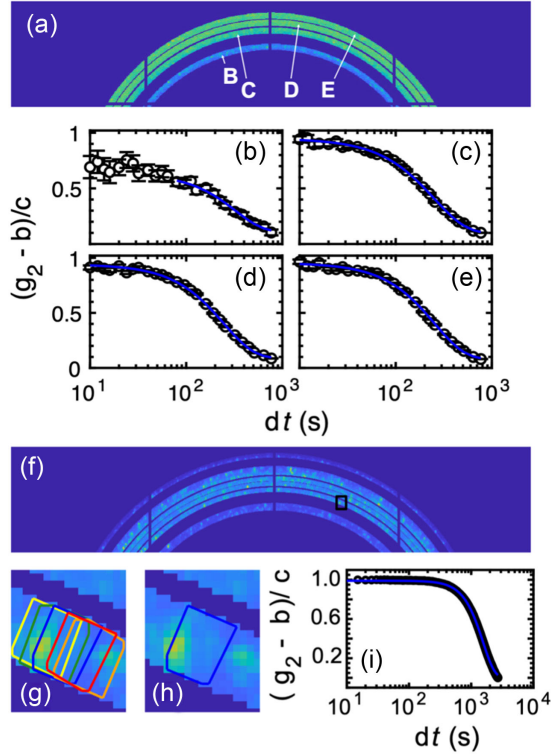
FIG. 2. Acceptance regions on the 2D detector used to generate $g_2(q, \varphi, dt)$ autocorrelation functions employed in this study. (a) Regions of the 2D detector used for XPCS analysis of the SB-B DDQC phase with (b)–(e) resulting autocorrelation functions $g_2(q, dt)$, from inner to outer Debye-Scherrer rings. (f) Regions of the 2D detector examined for XPCS analysis of the SB-B σ phase. (g) Azimuthal binning of σ Debye-Scherrer rings, with (h) one bin isolated for clarity and (i) its corresponding autocorrelation functions $g_2(q, \varphi, dt)$. Blue curves in (b)–(e), (h) are fits to Eq. (1).

presented in Figs. 2(b)–2(e), corresponding to the (00002), (12100), (01102), and (12101) reflections.

The $g_2(q, dt)$ functions were fit with a Kohlrausch-Williams-Watts (KWW) stretched exponential [31],

$$\frac{g_2(q, dt) - b}{c} = \exp\left(-2\left(\frac{dt}{\tau}\right)^{\beta}\right), \qquad (1)$$

with relaxation time τ, stretching exponent β, baseline b, and coherence c, as shown for the 135 °C DDQC dataset by blue curves in Figs. 2(b)–2(e).

In contrast to the azimuthally uniform scattering of the DDQC, the σ 2D-SAXS patterns exhibit considerable texture indicative of large coherent domains within the polycrystalline structure, which preclude conventional azimuthal averaging during autocorrelation analysis. Instead, evaluation of these XPCS data employed an analysis procedure recently reported by this group [24,25] for a polycrystalline bcc-forming SB diblock melt. Beyond localizing the XPCS analyses at q ranges centered on
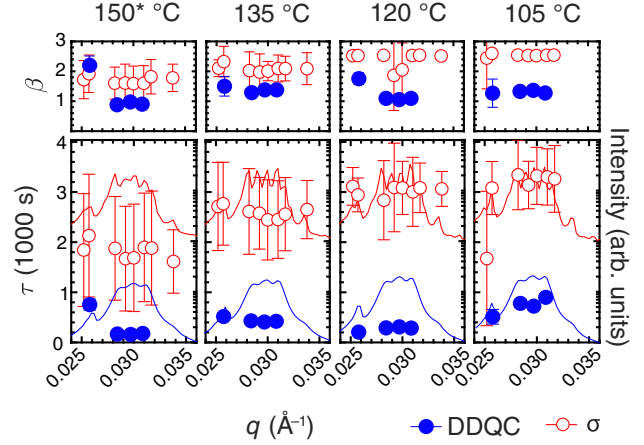

FIG. 3. Temperature- and q-dependent relaxation times (bottom) and stretching exponents (top) measured by XPCS for DDQC (solid blue points) and σ (open red points). 1D SAXS traces of the DDQC (bottom blue curve) and σ (top red curve) are provided for reference in the relaxation time panels. The "150* °C" label corresponds to σ data, the DDQC data in this panel was collected at 145 °C.

Debye-Scherrer rings ($\Delta q = 0.00075 \text{ Å}^{-1}$), this approach further decomposes each q ring into 750 partially overlapping φ bins ($\Delta\varphi \approx 1.2°$) to extract autocorrelation functions for separate Bragg spots associated with individual crystal grains. A set of five such bins is illustrated in Fig. 2(g), along with an enlargement of one bin [Fig. 2(h)] and its corresponding $g_2(q, \varphi, dt)$. As this curve is well described by the KWW function [Eq. (1)], the corresponding bin is classified as a "single relaxation." Similar fitting and sorting were executed for each of the 750 bins for each of the 8 reflections yielding a total of 6000 bins examined for the SB-B σ phase [25]. This binning analysis revealed that the σ phase produced numerous oscillating $g_2(q, \varphi, dt)$ functions known as heterodynes, attributed to optical mixing of x rays scattered from two sources moving relative to one another [35,37]. However, since >99% of the correlations observed in this work are single relaxations, the remainder of this report focuses on these types of bins. Additional information about σ phase heterodynes is given in Supplemental Material [27].

Application of Eq. (1) to the $g_2(q, dt)$ curves obtained from the DDQC and σ phases at 105, 120, 135, and (145) 150 °C yields τ and β values that are presented as a function of q in Fig. 3. Immediately apparent is the lack of q dependence of these τ's—for both structures. Notably, the temperature-dependent relaxation times $\tau = 1000$–3000 s observed for σ are considerably longer than those of the DDQC. Furthermore, in contrast to the DDQC ($\beta \approx 1.3$), compression exponents for σ tended to approach or exceed $\beta \approx 2.0$.

Also, the results in Fig. 3 reveal a modest temperature dependence of τ for both the DDQC and σ phases. For the DDQC, τ increases from $\tau \approx 200$ s to 500 s on cooling from

145 °C to 105 °C; lower temperature measurements were not feasible due to dynamical slowdown due to the glass transition temperature of the matrix block, $T_{g,S} \approx 100$ °C. Temperature-dependent τ values of the σ phase mirror this gradual increase in τ with decreasing temperature, approaching the full experiment timescale of 3600 s near 100 °C.

Intensity fluctuations in the reciprocal space map measured by XPCS at q_{hkl} corresponding to the respective DDQC and σ interplanar $\langle h_1 h_2 h_3 h_4 h_5 \rangle$ and $\langle hkl \rangle$ spacings and their associated relaxation times encode spatiotemporal fluctuations in these ordered mesocrystalline assemblies. The τ values deduced by our analyses lack any systematic Bragg plane symmetry dependence (Fig. 3). Thus, the dynamic processes measured by XPCS with $1 < \tau < 3000$ s do not occur along a preferred crystallographic axis. Since the axially symmetric σ and DDQC phases can be conceptualized as variations of the same square-triangle tiling motif as in Figs. 4(a) and 4(b) with nearly coincident (002) and (00002) c-axis spacings ($q = 0.026$ Å^{-1}) [8,18], the q-independent τ values rule out the possibility of specific interplanar spacing fluctuations associated with the propagation of symmetry-dependent phonon modes. Comparison of the dynamical timescales reveals a remarkable difference in τ in moving from 2D aperiodic order (DDQC) with $\tau \approx 500$ s to 3D periodic order (σ) with $\tau \approx 2500$ s illustrated in Fig. 3. This fact, coupled with the nearly identical coordination environments, particle radii ($R = 14.9$ nm, including particle core and corona), and volumetric particle densities in the two structures arising from the same sample, suggests that thermal motion (e.g., "rattling") of the particles in their coordination cages is not the source of the observed signal. We further discount phason dynamics, which are characterized by very long relaxation times [16].

Structural relaxations in the σ and DDQC assemblies could alternatively occur through intermicellar block copolymer chain exchange, due to the intrinsically reconfigurable nature of these soft particles [3,40]. However, the modest T dependences of the τ for both DDQC and σ (within a factor of 2) above T_g of the S block are inconsistent with the expected exponential temperature dependence of the chain exchange rate [40].

Instead, the slow relaxation times recorded for the DDQC and σ phase likely stem from grain boundary dynamics. Grain rotation and grain boundary diffusion have been previously invoked to rationalize dynamics measured by XPCS in diblock-copolymer lamellar phases [22] and bcc particle-forming diblock melts [24]. Induced by torques experienced by adjacent crystalline grains due to misorientation of the grain boundaries, grain rotation requires highly cooperative motion of many particles across large distances with a relatively large activation barrier [41]. However, grain boundary diffusion forgoes this need for cooperative motion and its associated activation energy is
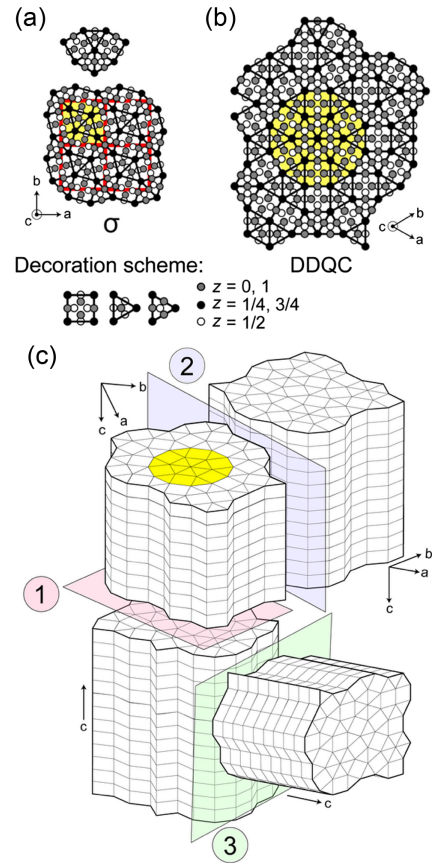

FIG. 4. 2D square and triangle tiling patterns of (a) σ and (b) DDQC phases in the (a),(b) plane and projected along the c axis. The three tiles used to construct each phase and the relative positions of particles decorating each tile are also shown. (c) Three types of DDQC grain boundaries associated with (1) grains with parallel periodic c axes but incommensurate stacking of the columns with aperiodic order in the a-b planes; (2) grains with coincident c-axis periodic order and incommensurate rotational symmetry in the a-b planes; and (3) grains with nonparallel c axes.

much lower. Consequently, we consider differences in the grain structures of the DDQC and σ phases of SB-B.

A Scherrer analysis [42] of the (002) and (00002) reflections in the σ and DDQC SAXS patterns, respectively, (Fig. 1 and [8]) indicates comparable extents of periodic order along the c axis ($>10d_{002}$ and $>10d_{00002}$, limited by instrument resolution). The numerous Bragg rings that exhibit "spotty" textures in the 3D-periodic σ phase SAXS patterns indicate the presence of large crystalline grains that coarsen on extended thermal annealing. These observations suggest that grain boundary formation in the σ phase is energetically costly. On the other hand, the isotropic and relatively limited number of Bragg rings obtained from the axially symmetric DDQC state suggest that this sample contains small aperiodically arranged columns of aperiodically ordered particles. This observation is consistent with earlier studies of diblock copolymers [8,43] and their

blends [26]. Both σ and DDQC crystal structures can be visualized as 2D tilings of decorated squares and triangles following a shared motif (Fig. 4). In this framework, σ comprises a single local arrangement of tiles, 3 triangles and 2 squares around a shared vertex [denoted $3^2.4.3.4$, Fig. 4(a)]. In contrast, real-space TEM imaging of diblock DDQCs reveals dodecagonal cogwheels interspersed within a disorganized 2D square-triangle tiling [Fig. 4(b)] [9], that nonetheless preserves local twelvefold rotational symmetry [44]. Thus, the energy associated with grain boundary formation in DDQCs is apparently relatively low. Since the particle packings in DDQC grain boundaries only need to conform to the local twelvefold symmetry with no translational symmetry, we speculate that the interfaces between the aperiodically ordered domains (grains) in the DDQC have a larger grain boundary width relative to the σ phase; representative grain configurations for the polycrystalline DDQC are depicted in Fig. 4(c). Thus, the larger grain boundary surface area arising from smaller grain sizes and larger grain boundary widths in the DDQC reduce particle confinement and enhance their mobility, as compared to the presumably narrower and more confining grain boundaries of the σ phase, in accord with the observed τ value trend [45,46].

Here, we note that the longer data acquisition time required to obtain acceptable XPCS counting statistics for σ (60 min) versus DDQC (16.7 min), and the significantly greater variance in the τ_σ values (Fig. 3), are consistent with the presence of much less grain boundary material in the σ versus DDQC specimen.

Figure 3 also illustrates an apparent shift in the β value through the DDQC $\to \sigma$ phase transition, wherein $\beta_{DDQC} \approx$ 1.3 and $\beta_\sigma \approx 2.0$. Whereas $\beta \approx 1$ suggests diffusive dynamics, $\beta > 1$ has been related to jamming transitions for disordered particle packings [47,48]. However, it is not yet clear how these principles translate to the grain dynamics of ordered materials. Structural heterogeneities in the local particle arrangements of the aperiodic DDQC implied by the apparently random square-triangle tiling possibly result in faster particle movement at grain boundaries, especially, relative to the σ phase that exhibits a structurally periodic tiling arrangement. Accordingly, grain boundary motion in σ may be highly restricted in a manner reminiscent of a jamming transition in a glass, which manifests as $\beta > 1$.

We report XPCS measurements of a single bidisperse SB-B blend sample, which forms both aperiodic DDQC and 3D-periodic σ phases on judicious thermal processing. Relaxation times for both structures, obtained from an identical sample, are independent of the scattering wavevector and weakly temperature dependent. Particle dynamics exhibited by the DDQC are 5 times faster than for σ, which is ascribed to differences in their grain boundary structures and dynamics. These results expose a new approach for exploiting XPCS to characterize particle dynamics in ordered soft materials, a technique that will be broadly available to the condensed matter physics community with the advent of upgraded synchrotron user facilities that offer access to greatly enhanced x-ray beam brilliance and coherence.

The authors declare no competing financial interest.

---

[*]Corresponding author: maheshkm@umn.edu
[†]Corresponding author: bates001@umn.edu

[1] R. Vargas, P. Mariani, A. Gulik, and V. Luzzati, Cubic phases of lipid-containing systems: The structure of phase Q^{223} (space group $Pm3(-)n$). An x-ray scattering study, J. Mol. Biol. **225**, 137 (1992).

[2] G. Ungar, Y. Liu, X. Zeng, V. Percec, and W.-D. Cho, Giant supramolecular liquid crystal lattice, Science **299**, 1208 (2003).

[3] S. Lee, C. Leighton, and F. S. Bates, Sphericity and symmetry breaking in the formation of Frank-Kasper phases from one component materials, Proc. Natl. Acad. Sci. U.S.A. **111**, 17723 (2014).

[4] M. W. Bates, J. Lequieu, S. M. Barbon, R. M. Lewis, K. T. Delaney, A. Anastasaki, C. J. Hawker, G. H. Fredrickson, and C. M. Bates, Stability of the A15 phase in diblock copolymer melts, Proc. Natl. Acad. Sci. U.S.A. **116**, 13194 (2019).

[5] S. A. Kim, K.-J. Jeong, A. Yethiraj, and M. K. Mahanthappa, Low-symmetry sphere packings of simple surfactant micelles induced by ionic sphericity, Proc. Natl. Acad. Sci. U.S.A. **114**, 4072 (2017).

[6] Z. Su et al., Identification of a Frank-Kasper Z phase from shape amphiphile self-assembly, Nat. Chem. **11**, 899 (2019).

[7] X. Zeng, G. Ungar, Y. Liu, V. Percec, A. E. Dulcey, and J. K. Hobbs, Supramolecular dendritic liquid quasicrystals, Nature (London) **428**, 157 (2004).

[8] T. M. Gillard, S. Lee, and F. S. Bates, Dodecagonal quasicrystalline order in a diblock copolymer melt, Proc. Natl. Acad. Sci. U.S.A. **113**, 5167 (2016).

[9] A. P. Lindsay, R. M. Lewis, III, B. Lee, A. J. Peterson, T. P. Lodge, and F. S. Bates, A15, σ, and a quasicrystal: Access to complex particle packings via bidisperse diblock copolymer blends, ACS Macro Lett. **9**, 197 (2020).

[10] A. Jayaraman, C. M. Baez-Cotto, T. J. Mann, and M. K. Mahanthappa, Dodecagonal quasicrystals of oil-swollen ionic surfactant micelles, Proc. Natl. Acad. Sci. U.S.A. **118,** e2101598118 (2021).

[11] K. Yue *et al.*, Geometry induced sequence of nanoscale Frank-Kasper and quasicrystal mesophases in giant surfactants, Proc. Natl. Acad. Sci. U.S.A. **113,** 14195 (2016).

[12] D. Shechtman, I. Blech, D. Gratias, and J. W. Cahn, Metallic phase with long-range orientational order and no translational symmetry, Phys. Rev. Lett. **53,** 1951 (1984).

[13] D. Levine and P. J. Steinhardt, Quasicrystals: A new class of ordered structures, Phys. Rev. Lett. **53,** 2477 (1984).

[14] A. I. Goldman and R. F. Kelton, Quasicrystals and crystalline approximants, Rev. Mod. Phys. **65,** 213 (1993).

[15] I. Han, K. L. Wang, A. T. Cadotte, Z. Xi, H. Parsamehr, X. Xiao, S. C. Glotzer, and A. J. Shahani, Formation of a single quasicrystal upon collision of multiple grains, Nat. Commun. **12,** 5790 (2021).

[16] K. Edagawa, K. Suzuki, and S. Takeuchi, High resolution transmission electron microscopy observation of thermally fluctuating phasons in decagonal Al-Cu-Co, Phys. Rev. Lett. **85,** 1674 (2000).

[17] S. Iwami and T. Ishimasa, Dodecagonal quasicrystal in Mn-based quaternary alloys containing Cr, Ni, and Si, Philos. Mag. Lett. **95,** 229 (2015).

[18] G. Ungar and X. Zeng, Frank-Kasper, quasicrystalline and related phases in liquid crystals, Soft Matter **1,** 95 (2005).

[19] A. J. Patel, S. Narayanan, A. Sandy, S. G. J. Mochrie, B. A. Garetz, H. Watanabe, and N. P. Balsara, Relationship between structural and stress relaxation in a block-copolymer melt, Phys. Rev. Lett. **96,** 257801 (2006).

[20] A. Sanz, T. A. Ezquerra, R. Hernández, M. Sprung, and A. Nogales, Relaxation processes in a lower disorder order transition diblock copolymer, J. Chem. Phys. **142** (2015).

[21] W.-S. Jang, P. Koo, M. Sykorsky, S. Narayanan, A. Sandy, and S. G. J. Mochrie, The static and dynamic structure factor of a diblock copolymer melt via small-angle x-ray scattering and x-ray photon correlation spectroscopy, Macromolecules **46,** 8628 (2013).

[22] O. Oparaji, S. Narayanan, A. Sandy, S. Ramakrishnan, and D. Hallinan, Jr., Structural dynamics of strongly segregated block copolymer electrolytes, Macromolecules **51,** 2591 (2018).

[23] R. M. Lewis, III, H. K. Beech, G. L. Jackson, M. J. Maher, K. Kim, S. Narayanan, T. P. Lodge, M. K. Mahanthappa, and F. S. Bates, Dynamics of a supercooled disordered sphere-forming diblock copolymer as determined by x-ray photon correlation and dynamic mechanical spectroscopies, ACS Macro Lett. **7,** 1486 (2018).

[24] R. M. Lewis, III, G. L. Jackson, M. J. Maher, K. Kim, S. Narayanan, T. P. Lodge, M. K. Mahanthappa, and F. S. Bates, Grain growth and coarsening dynamics in a compositionally asymmetric block copolymer revealed by x-ray photon correlation spectroscopy, Macromolecules **53,** 8233 (2020).

[25] R. M. Lewis, III, G. L. Jackson, M. J. Maher, K. Kim, T. P. Lodge, M. K. Mahanthappa, S. Narayanan, and F. S. Bates, A new framework for x-ray photon correlation spectroscopy analysis from polycrystalline materials, Rev. Sci. Instrum. **89** (2018).

[26] A. P. Lindsay, G. K. Cheong, A. J. Peterson, S. Weigand, K. D. Dorfman, T. P. Lodge, and F. S. Bates, Complex phase behavior in particle-forming AB/AB′ diblock copolymer blends with variable core block lengths, Macromolecules **54,** 7088 (2021).

[27] See Supplemental Material at http://link.aps.org/supplemental/10.1103/PhysRevLett.132.158101, which includes Refs. [28–37], for complete binary diblock-copolymer blend phase diagram, XPCS sample stability analyses, data reduction and fitting details, and representative time correlations and their classifications.

[28] A. J. F. Siegert, *On the fluctuations in signals returned by many independently moving scatterers* (Radiation Laboratory, Massachusetts Institute of Technology, Cambridge, MA, 1943).

[29] D. Ferreira, R. Bachelard, W. Guerin, R. Kaiser, and M. Fouché, Connecting field and intensity correlations: The Siegert relation and how to test it, Am. J. Phys. **88,** 831 (2020).

[30] R. Kohlrausch, Theorie des elektrischen Rückstandes in der Leidener flasche, Ann. Phys. (N.Y.) **167,** 179 (1854).

[31] J. C. Phillips, Stretched exponential relaxation in molecular and electronic glasses, Rep. Prog. Phys. **59,** 1133 (1996).

[32] R. A. Narayanan, P. Thiyagarajan, S. Lewis, A. Bansal, L. S. Schadler, and L. B. Lurio, Dynamics and internal stress at the nanoscale related to unique thermomechanical behavior in polymer nanocomposites, Phys. Rev. Lett. **97,** 075505 (2006).

[33] C. Caronna, Y. Chushkin, A. Madsen, and A. Cupane, Dynamics of nanoparticles in a supercooled liquid, Phys. Rev. Lett. **100,** 055702 (2008).

[34] S. Srivastava, L. A. Archer, and S. Narayanan, Structure and transport anomalies in soft colloids, Phys. Rev. Lett. **110,** 148302 (2013).

[35] J. R. M. Lhermitte, M. C. Rogers, S. Manet, and M. Sutton, Velocity measurement by coherent x-ray heterodyning, Rev. Sci. Instrum. **88** (2017).

[36] J. G. Ulbrandt, M. G. Rainville, C. Wagenbach, S. Narayanan, A. R. Sandy, H. Zhou, K. F. Ludwig Jr, and R. L. Headrick, Direct measurement of the propagation velocity of defects using coherent x-rays, Nat. Phys. **12,** 794 (2016).

[37] F. Livet, F. Bley, F. Ehrburger-Dolle, I. Morfin, E. Geissler, and M. Sutton, X-ray intensity fluctuation spectroscopy by heterodyne detection, J. Synchrotron Radiat. **13,** 453 (2006).

[38] K. Schatzel, Noise on photon correlation data. I. Autocorrelation functions, Quantum Opt. **2,** 287 (1990).

[39] L. Cipelletti and D. A. Weitz, Ultralow-angle dynamic light scattering with a charge coupled device camera based multispeckle, multitau correlator, Rev. Sci. Instrum. **70,** 3214 (1999).

[40] K. A. Cavicchi and T. P. Lodge, Domain size equilibration in sphere-forming block copolymers, J. Polym. Sci., Part B: Polym. Phys. **41,** 715 (2003).

[41] D. Moldovan, D. Wolf, and S. R. Phillpot, Theory of diffusion-accommodated grain rotation in columnar polycrystalline microstructures, Acta Mater. **49,** 3521 (2001).

[42] A. L. Patterson, The Scherrer formula for x-ray particle size determination, Phys. Rev. **56,** 978 (1939).

[43] A. J. Mueller, A. P. Lindsay, A. Jayaraman, T. P. Lodge, M. K. Mahanthappa, and F. S. Bates, Quasicrystals and their approximants in a crystalline-amorphous diblock copolymer, Macromolecules **54**, 2647 (2021).

[44] M. Oxborrow and C. L. Henley, Random square-triangle tilings: A model for twelvefold-symmetric quasicrystals, Phys. Rev. B **48**, 6966 (1993).

[45] H. Zhang, D. J. Srolovitz, J. F. Douglas, and J. A. Warren, Grain boundaries exhibit the dynamics of glass-forming liquids, Proc. Natl. Acad. Sci. U.S.A. **106**, 7735 (2009).

[46] K. H. Nagamanasa, S. Gokhale, R. Ganapathy, and A. K. Sood, Confined glassy dynamics at grain boundaries in colloidal crystals, Proc. Natl. Acad. Sci. U.S.A. **108**, 11323 (2011).

[47] L. Cipelletti, L. Ramos, S. Manley, E. Pitard, D. A. Weitz, E. E. Pashkovski, and M. Johansson, Universal non-diffusive slow dynamics in aging soft matter, Faraday Discuss. **123**, 237 (2003).

[48] S. Srivastava, P. Agarwal, R. Mangal, D. L. Koch, S. Narayanan, and L. A. Archer, Hyperdiffusive dynamics in Newtonian nanoparticle fluids, ACS Macro Lett. **4**, 1149 (2015).